

Cosmic microwave anisotropies from BPS semilocal strings

Jon Urrestilla,^{1,*} Neil Bevis,^{2,1,†} Mark Hindmarsh,^{1,‡} Martin Kunz,^{3,1,§} and Andrew R. Liddle^{1,¶}

¹*Department of Physics & Astronomy, University of Sussex, Brighton, BN1 9QH, United Kingdom*

²*Theoretical Physics, Blackett Laboratory, Imperial College, London, SW7 2BZ, United Kingdom*

³*Département de Physique Théorique, Université de Genève, 1211 Genève 4, Switzerland*

(Dated: 11/07/2008)

We present the first ever calculation of cosmic microwave background (CMB) anisotropy power spectra from semilocal cosmic strings, obtained via simulations of a classical field theory. Semilocal strings are a type of non-topological defect arising in some models of inflation motivated by fundamental physics, and are thought to relax the constraints on the symmetry breaking scale as compared to models with (topological) cosmic strings. We derive constraints on the model parameters, including the string tension parameter μ , from fits to cosmological data, and find that in this regard BPS semilocal strings resemble global textures more than topological strings. The observed microwave anisotropy at $\ell = 10$ is reproduced if $G\mu = 5.3 \times 10^{-6}$ (G is Newton's constant). However as with other defects the spectral shape does not match observations, and in models with inflationary perturbations plus semilocal strings the 95% confidence level upper bound is $G\mu < 2.0 \times 10^{-6}$ when CMB data, Hubble Key Project and Big Bang Nucleosynthesis data are used (c.f. $G\mu < 0.9 \times 10^{-6}$ for cosmic strings). We additionally carry out a Bayesian model comparison of several models with and without defects, showing models with defects are neither conclusively favoured nor disfavoured at present.

I. INTRODUCTION

Recent observational data are tightly constraining cosmological models, in many cases rendering them non-viable. One of the constraints comes from the fact that many potentially successful high-energy physics motivated models of inflation predict a cosmic string network [1, 2] in the post-inflationary era: this occurs in supersymmetric hybrid inflation [3], in grand unified theories [4] and in some string theory inflation models [5, 6, 7, 8]. These strings and other type of defects contribute to the cosmic microwave background (CMB) anisotropies in addition to the primordial inflationary fluctuations, allowing CMB experiments to provide upper limits on the contribution from defects [9, 10, 11, 12, 13]. In the near future, observations will either reveal the presence of these defects or will significantly tighten the constraints upon the models from which they are predicted (see for example Refs. [14, 15, 16, 17, 18]).

However, a simple and elegant method for evading the constraints coming from cosmic strings in these models was proposed in Refs. [19, 20]. A duplication of the matter fields responsible for the string formation, which arises quite naturally in several models [20, 21, 22], changes the nature of the strings from topological and therefore long-lived strings, to non-topological semilocal strings [23]. All the desired inflationary properties of the model persist, and semilocal strings are believed to be

cosmologically less harmful than their topological counterparts, in that their energy density may be lower for a given symmetry breaking scale. In this paper we confirm these expectations by performing the first CMB calculations for semilocal strings and determine the constraints upon semilocal strings imposed by current data.

Calculating the additional contribution that cosmic strings would make to the CMB temperature and polarization power spectra is not an easy task. They are highly non-linear entities, and the range of scales involved in the problem is enormous. However, as the width of the string is much smaller than the string length, one possibility is to neglect the finite width and perform Nambu–Goto type simulations [24, 25, 26, 27]. Unfortunately, these simulations ignore the string decay into gravitational waves or particles and the corresponding back-reaction onto the network. Their representation of small-scale loop production in the network is also under debate [28, 29, 30, 31, 32]. Yet another level of simplification often used in CMB calculations for local strings is to simulate merely a stochastic ensemble of unconnected string segments [10, 11, 14, 16, 33, 34]. Lacking any dynamical equations, in this case the sub-horizon decay of strings must be taken into account by the random removal of segments, at a rate chosen to match that seen in network simulations, but qualitatively accurate results are obtained with much less computational cost. In the global defect case, the energy is not localized into the string cores and their resolution is not essential. This enables the calculation of CMB contributions from global defects using field theory simulations [35, 36].

None of these three approaches is useful for the study of semilocal strings, since they are not well-modelled by Nambu–Goto strings while, unlike the global case, the string cores are potentially important. Fortunately, in a recent breakthrough we performed the first CMB cal-

*Electronic address: j.urrestilla@sussex.ac.uk

†Electronic address: n.bevis@imperial.ac.uk

‡Electronic address: m.b.hindmarsh@sussex.ac.uk

§Electronic address: martin.kunz@physics.unige.ch

¶Electronic address: a.liddle@sussex.ac.uk

culations for local cosmic strings to derive from field-theoretical simulations [37]. We achieved this by the use of a parametrized approximation to reduce the range of scales required in the simulations, but which had no resolvable effect on the CMB predictions. That approach has opened the door for the possibility of simulating defects with no known approximating models.

We have therefore employed the machinery developed for the local string case to the simplest model containing semilocal strings, with the parameters chosen to give the Bogomol'nyi–Prasad–Sommerfield (BPS) limit (see Section II). The BPS limit arises naturally in D-term SUSY inflation and $D3/D7$ brane inflation. We leave the study of non-BPS cases to a future article but it is the expectation that in the two opposite extremes between which the BPS case lies, the semilocal result will tend to that of global textures or to that of local strings [38, 39, 40]. We perform a detailed comparison of our results with these two cases using our earlier results in Ref. [37] for local strings. For the case of global textures, we perform CMB calculations using the linear σ model.¹ We leave a discussion of our texture calculations to an Appendix.

We have also performed a multi-parameter comparison with current data, yielding results similar to those of Ref. [13] where it was seen that local cosmic strings are mildly favoured by current CMB data. We find that the preference for semilocal strings is slightly greater and, as in Ref. [13], we explore this preference using Bayesian evidence calculations, as well as considering the implications of non-CMB data.

This paper is organized as follows: in the next Section we discuss the semilocal string model, before giving a brief overview of the simulation and CMB calculation method in Section III. We will then present our CMB results and consistency checks in Section IV, including the comparison with local strings and global textures. Section V then presents the comparison with data.

II. SEMILOCAL STRING MODEL

The simplest model giving rise to semilocal strings is given by the Lagrangian density [23]

$$\mathcal{L} = |D_\mu\phi_1|^2 + |D_\mu\phi_2|^2 - \frac{1}{4e^2}F_{\mu\nu}F^{\mu\nu} - \frac{\lambda}{4}\left(|\phi_1|^2 + |\phi_2|^2 - \eta^2\right)^2, \quad (1)$$

where $D_\mu = \partial_\mu + iA_\mu$ and $F_{\mu\nu} = \partial_\mu A_\nu - \partial_\nu A_\mu$. The fields ϕ_1 and ϕ_2 are complex scalar fields and A_μ is an Abelian gauge field. The parameter η gives the symmetry breaking scale. This Lagrangian possesses all the necessary ingredients to give rise to semilocal strings and so allows

insight into more complicated models, such as D-term inflation in $N = 1$ or $N = 2$ supersymmetric (SUSY) models [42, 43] and $D3/D7$ brane inflation [20].

Since this model is just the Abelian Higgs model with an extra Higgs field, the semilocal strings arising from it can be seen as embedded Nielsen–Olesen strings [44]. The vacuum manifold is S^3 , which is simply connected, and the existence and stability of the strings depend on energetic and dynamical causes, not on the topology of the vacuum. There is only one parameter governing the stability of the strings, namely, $\beta^2 \equiv \lambda/2e^2$: for $\beta < 1$ they are stable (even quantum mechanically); for $\beta > 1$ they are unstable. The BPS case ($\beta = 1$) is the transitional case, where the strings are neutrally stable [45, 46]. There is a zero mode concerning the string width in the BPS case: all strings with widths that range from the width of an Abelian Higgs string to infinity are degenerate in energy. But even though the string can have a very large (infinite) core, the magnetic flux is nevertheless quantized. It is also worth noting that when two semilocal strings of any width collide, they intercommute [47, 48, 49] and their widths may revert to the minimum width (i.e., the width of an Abelian Higgs string) [48]. As mentioned earlier, the BPS case arises naturally in, for example, D-term inflationary scenarios. In more generic cases, non-BPS cases will arise. We can anticipate some qualitative behaviour for the non-BPS case. For $\beta > 1$ the semilocal string become unstable, and they will behave like global textures. For $\beta < 1$, the lower the value of β , the more semilocal string networks resemble Abelian Higgs string networks [40], and their CMB predictions will tend to that of Abelian Higgs strings.

One important difference between Abelian Higgs cosmic strings and semilocal strings is that the latter are non-topological, so they can have ends. We therefore do not expect infinite semilocal strings to be formed by the Kibble mechanism in a cosmological phase transition. Instead, a collection of segments forms. The evolution of the segments is very complicated: some will shrink to zero, others will join both ends to form loops, while some will join to nearby segments to make longer segments, and eventually form virtually infinite strings [40]. At the BPS limit, the formation of longer segments is strongly suppressed, which led the authors of Refs. [19, 20] to conjecture that no strings would be formed in such a model after inflation, and to claim that the D-term inflation without cosmic strings could take place.

While the semilocal model can be reduced to the Abelian Higgs model by removing one complex scalar field, it can also be reduced to a global texture model by removing the gauge field (see Appendix). A key question is how those removals modify the predicted anisotropy, keeping fundamental Lagrangian parameters fixed. An important derived parameter is the string mass per unit length in the Abelian Higgs and semilocal cases [44, 50]:

$$\mu \equiv 2\pi\eta^2, \quad (2)$$

and the CMB anisotropies are proportional $(G\mu)^2$, where

¹ See for instance Ref. [41] for a comparison of the dynamics of the linear and non-linear σ models.

G is the gravitational constant. We continue to use this measure even when talking about the texture model, but in that case it has no direct interpretation and is merely a measure of the energy scale of the model. It is known that textures give significantly lower anisotropies than strings for a given $G\mu$, since textures decay much more quickly once inside the horizon. Our original preconception was that the anisotropies from semilocal strings would be of the same order as, but a little smaller than, those of textures. This expectation is because the gauge field cancels some of the field gradients present in the texture case and contributes little to the energy density [46], while in the BPS limit there are no long strings and hence no expectation of large anisotropies from string-like sources. Indeed, we will find that this expectation is confirmed by our detailed analysis.

III. CMB CALCULATION METHOD

A. Overview

As discussed in the introduction, the method used to calculate CMB power spectra employed here is exactly that used for Abelian Higgs strings in Ref. [37] and we refer the interested reader to that article for greater depth. However we will briefly describe the fundamentals of the approach in this Section.

Since observations reveal that the cosmological perturbations are small (except on short scales in the current epoch) the defects can be taken to evolve in an expanding flat Friedmann–Lemaître–Robertson–Walker universe. Inflation is taken to set up small primordial fluctuations, which then evolve passively under the Einstein–Boltzmann equations. However, the defects perturb the metric, via their energy–momentum tensor, and these perturbations also have to be taken into account when computing CMB power spectra. But since the perturbations introduced by either inflation or defects are very small, any coupling between them is insignificant and the two perturbation sets may be calculated separately. The result is two statistically independent sets of CMB anisotropies, the power spectra of which simply add to give the total.

Fundamentally the CMB power spectra are two-point correlation functions of the CMB temperature (or polarization) fluctuations, and in the defect case they can be determined from the two-point unequal-time correlation functions (UETCs) of the defect energy–momentum tensor $\tilde{T}_{\mu\nu}$ [35, 51, 52, 53]:

$$\tilde{U}_{\kappa\lambda\mu\nu}(\mathbf{k}, \tau, \tau') = \left\langle \tilde{T}_{\kappa\lambda}(\mathbf{k}, \tau) \tilde{T}_{\mu\nu}^*(\mathbf{k}, \tau') \right\rangle. \quad (3)$$

Here \mathbf{k} is the comoving wavevector, τ and τ' are two conformal times and \sim denotes a Fourier space quantity, as in the notation of Ref. [37].

However, the above 55 complex functions of 3 variables may be reduced to just 5 real functions of two variables,

via the use of statistical isotropy, energy–momentum conservation, and a property of defect networks known as *scaling*. The last property derives from the causal nature of the network: that field smoothing is limited by the horizon and, as such, defect networks often tend to an attractor regime in which statistical measures of their distribution are a function of a single quantity: the horizon size τ . Assuming scaling and statistical isotropy, the UETCs can be written as [53, 37]

$$\tilde{U}_{\kappa\lambda\mu\nu}(k, \tau, \tau') = \frac{\eta^4}{\sqrt{\tau\tau'}} \frac{1}{V} \tilde{C}_{\kappa\lambda\mu\nu}(k\tau, k\tau') \quad (4)$$

where V is the fiducial simulation volume and \tilde{C} is the scaling function of the UETC. Further, the functions \tilde{C} decay for large or small τ/τ' or for large $k\sqrt{\tau\tau'}$ and hence their measurement is only required over a fairly limited parameter space.

Of the 5 independent scaling functions, 3 of them represent scalar degrees of freedom ($\tilde{C}_{11}^S(k\tau, k\tau')$, $\tilde{C}_{12}^S(k\tau, k\tau')$, $\tilde{C}_{22}^S(k\tau, k\tau')$) while the remaining two represent the vector and tensor degrees of freedom respectively ($\tilde{C}^V(k\tau, k\tau')$, $\tilde{C}^T(k\tau, k\tau')$) [37, 52]. Unlike the inflationary case, the amplitude of the tensor perturbations is fixed and directly obtained from the simulations, and it is not possible to neglect the vector perturbations as they are continuously sourced by the presence of the defect network.

The UETC scaling functions are then fed into a modified version of the CMBEASY Boltzmann code [54] which computes the CMB temperature and polarization power spectra. However, in order for CMBEASY to use the UETC data, the functions $\tilde{C}(k\tau, k\tau')$ must be first decomposed as:

$$\tilde{C}(k\tau, k\tau') = \sum_n \lambda_n \tilde{c}_n(k\tau) \tilde{c}_n(k\tau'), \quad (5)$$

which in the numerical case is tantamount to determining the eigenvalues and eigenvectors of a real, symmetric matrix. Note that \tilde{C}_{12}^S is not symmetric, but $\tilde{C}_{21}^S(k\tau, k\tau') = \tilde{C}_{12}^S(k\tau', k\tau)$ and so the $M \times M$ matrices representing the scalar degrees of freedom ($\tilde{C}_{11}^S, \tilde{C}_{12}^S, \tilde{C}_{21}^S$ and \tilde{C}_{22}^S) are tiled together to yield a symmetric $2M \times 2M$ matrix which is then decomposed this way.

The modified CMBEASY then takes a single eigenvector \tilde{c}_n as a source function and determines the corresponding contribution to the CMB power spectra, with summation over all such contributions yielding the total. We found that for the semilocal case, the number of eigenvectors that should be included in the computation of the power spectra to achieve convergence was lower than that needed in the Abelian Higgs case; nevertheless, we use the same number of eigenvectors as in the Abelian Higgs case (see Table I) to minimize the differences in the computation. Also there are some choices about how to decompose the UETCs into the form of Eq. (5), and again we follow exactly the method of Ref. [37].

Note that scaling is broken at the radiation–matter transition and therefore the scaling UETC functions must be determined for the defects under both matter and radiation-domination. These are decomposed into eigenvectors and fed into the modified CMBEASY code, which then interpolates between the radiation and matter results to model the transition. For the transition into the Λ -dominated epoch, the sources simply decay and simulation is not required. In any case, perturbations sourced at such late times affect only the very largest scales.

B. Semilocal simulations

In order to calculate the scaling UETC functions for the semilocal string model above, we perform field theory simulations under both radiation- and matter-domination. However, since at times of importance for CMB calculations the string width is many orders of magnitude smaller than the horizon size, it is not possible to perform simulations for such times while still resolving the string cores. Fortunately, scaling implies that this is not required and that the scaling UETC functions may be obtained from simulations of early times, with $\tau \sim 100\eta^{-1}$, and then used to describe the late-time behaviour of the system. Note that although we perform simulations in a matter-dominated background for $\tau \sim 100\eta^{-1}$, when the real universe was radiation-dominated, scaling implies that the network properties are the same at $100\eta^{-1}$ as they are in the true late-time matter era.

However, performing the simulations required with current or near future computational technology is a considerable challenge. The (minimum) string width (r_{\min}) is fixed in physical coordinates and, in the comoving coordinates required for the simulations, it varies as:

$$r_{\min} = \frac{1}{a\sqrt{\lambda}\eta} = \frac{1}{2ae\eta}, \quad (6)$$

where a is the cosmic scale factor. It therefore shrinks as τ^{-1} under a radiation- or as τ^{-2} under a matter-dominated universe. If the strings are resolved at the end of the simulation, then they are enormous and larger than the horizon size for times only a little earlier, particularly under matter domination. The system will not scale, or even contain significant regions where the fields lie on the vacuum manifold, if τ is comparable to r_{\min} . Thus, the UETC data can only be collected over a limited region of the required parameter space.

A simple means of circumventing the above problem is to promote the parameters λ and e in the action to time-dependent variables [37] as:

$$\begin{aligned} \lambda &= \lambda_0 a^{-2(1-s)} \\ e &= e_0 a^{-(1-s)}. \end{aligned} \quad (7)$$

Now the scale r_{\min} varies as:

$$r_{\min} = r_{\min,0} a^{-s}, \quad (8)$$

and variation of the action yields equations of motion as:

$$\begin{aligned} \ddot{\phi}_1 + 2\frac{\dot{a}}{a}\dot{\phi}_1 - D_j D_j \phi_1 &= -a^{2s} \frac{\lambda_0}{2} (|\phi_1|^2 + |\phi_2|^2 - \eta^2) \phi_1 \\ \ddot{\phi}_2 + 2\frac{\dot{a}}{a}\dot{\phi}_2 - D_j D_j \phi_2 &= -a^{2s} \frac{\lambda_0}{2} (|\phi_1|^2 + |\phi_2|^2 - \eta^2) \phi_2 \\ \dot{F}_{0j} + 2(1-s)\frac{\dot{a}}{a}F_{0j} - \partial_i F_{ij} &= \\ &= -2a^{2s} e_0^2 \mathcal{I}m[\phi_1^* D_j \phi_1 + \phi_2^* D_j \phi_2]. \end{aligned} \quad (9)$$

For the case of $s = 1$, the true dynamics are obtained, while for $s = 0$ the factors of a responsible for the shrinkage of the (minimum) string width are removed from the equations of motion and r_{\min} becomes comoving. This is similar to methods of Refs. [55, 56], where the undesirable factors of a were directly removed from the dynamical equations, but here the parameter s can be varied and its effects measured. This is particularly important because $s \neq 1$ means that energy–momentum conservation is violated and it is $T_{\mu\nu}$ that sources the perturbations. For the simulations under radiation-domination we can actually simulate the $s = 1$ case directly and compare in detail our intermediate results for $s < 1$ with the true case. However, one of the results of Ref. [37] was that the CMB results for Abelian Higgs strings are insensitive to s , and here we extend that result to semilocal strings.

There is good evidence from previous simulations of both Abelian Higgs and semilocal strings that the network results are independent of the initial conditions once scaling is reached [39, 56, 57, 58, 37]. The goal is therefore to produce an initial configuration in a numerically feasible way that obeys the analogue of Gauss’ law in the model and that will yield scaling fairly fast, in order to maximize the dynamical range of the simulation. Following again Ref. [37] we set all temporal derivatives and gauge fields to zero, and the fields ϕ_1 and ϕ_2 are set in such a way that they lie in the vacuum manifold ($|\phi_1|^2 + |\phi_2|^2 = \eta^2$) with random phases in S^3 . The system is then evolved using the equations of motion obtained after discretizing the action via the standard Moriarty et al. [59] scheme and encoded in C++ using the LATfield Library [60]. This scheme preserves the Gauss constraint during the evolution, even in the case of $s < 1$, because our equations are derived from the discretized action (see Ref. [37]).

IV. SIMULATION AND CMB POWER SPECTRUM RESULTS

A. Numerical aspects and tests for scaling

The numerical simulations were performed on the UK National Cosmology Supercomputer [61], where we simulated five different realizations for both matter- and radiation-dominated epochs and for $s = 0.0$ and $s = 0.3$, as well as $s = 1$ for radiation alone. Of those, only the simulations with $s = 0.3$ were used to produce the CMB

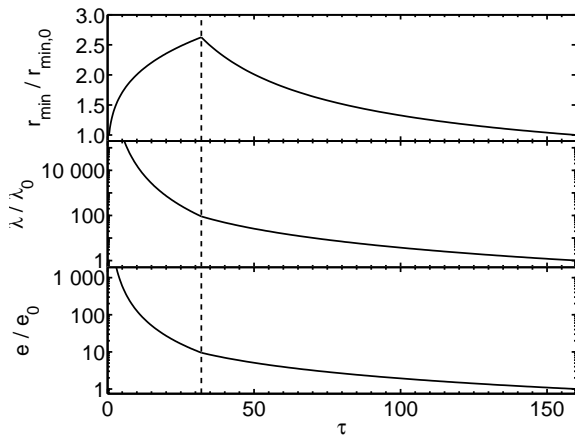


FIG. 1: Variation of r_{\min} and the parameters e and λ for the $s = 0.3$ simulations, which mimic the one used in Ref. [37]. The subscript 0 denotes the value at the end of the simulation.

Parameter	Value
Lattice size N	512
Lattice spacing Δx [η^{-1}]	0.5
Time-step Δt [η^{-1}]	0.1
Scalar coupling λ_0	2.0
Gauge coupling e_0	1.0
Initial conformal time τ_i [η^{-1}]	1.0
Final conformal time τ_{end} [η^{-1}]	128
Initial s	-0.116
Final s	0.3
Time of change in s value [η^{-1}]	32
τ_{sim} range of ξ fit [η^{-1}]	50 - 128
Dynamic range $(\tau/\tau')_{\text{max}}$	~ 2
UETC sample matrix size	512
UETC matrix sampling	linear
No. eigenvectors	128

TABLE I: Parameters used in production runs. The first part of the table lists the parameters of the simulations, with the second part listing parameters of the UETC method for calculating the CMB power spectrum. Note that the values are identical to those of Ref. [37], except for the time range of the simulations.

power spectra; the others were used to test the validity of our approach. We begin and end the simulation with the same value for r_{\min} ; that is, we initially set s to a negative value so that r_{\min} increases until a time τ_s , after which s is positive so that r_{\min} shrinks during the primary part of the simulation (see Fig.1). This process accelerates the formation of vacuum regions.

Table I shows the values of the parameters used for the production runs. Most of the parameters match those of Ref. [37]; furthermore, the coupling parameters were also varied as shown in Fig. 1 to replicate the behaviour of Ref. [37]. Because of the existence of zero modes in the semilocal system it is dangerous to run the simulation for

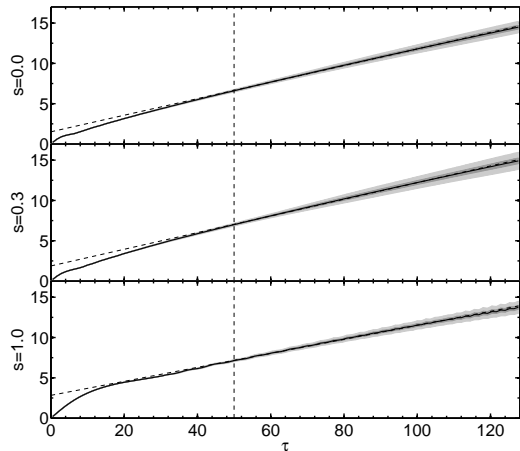


FIG. 2: Average value of ξ , as defined in Eq. (10), for $s = 0.0, 0.3, 1.0$, in the radiation era. The average is over five different realizations for each value of s , and the shaded regions correspond to $1\text{-}\sigma$ and $2\text{-}\sigma$ deviations. The best-fit line for times $\tau > 50$ is also shown (dashed line). Note that the best-fit line is an excellent approximation, and that the differences between different values of s are minimal.

longer than the half-crossing-time. In order to keep the dynamic range of Ref. [37], here we had to begin taking UETC data at an earlier time ($\tau = 50$ rather than $\tau = 64$). One might wonder whether the system is already into the scaling regime by those early times, but we will show in this Section that in fact this is the case.

One means to test for scaling is via the string length density, which should be proportional to τ^{-2} , since the average length of string per horizon volume should be proportional to τ and the horizon volume varies as τ^3 . The detection of (topological) Abelian Higgs strings in a lattice field simulation is fairly straightforward, since one can track, for instance, zeros of the Higgs field or the winding of its phase around them. Alternatively one could use the average Lagrangian density (as in Ref. [37]) or the T_{00} component of the energy-momentum tensor, which should also vary as τ^{-2} .

In fact, for (non-topological) semilocal strings those alternative methods must be employed: the zeros of the Higgs fields are not a good measure, since there is no need for the string core to be a zero of the Higgs field. Besides, semilocal strings in the Bogomol'nyi limit ($\beta = 1$) are expected to form short segments that either collapse very quickly or become fatter, diluting away the core of the string. That is why we used a different measure to quantify the scaling of the semilocal BPS string system.

In this work, we use the T_{00} component of the energy-momentum tensor to define our length measure ξ as:

$$\xi = \frac{\eta}{\sqrt{T_{00}}}, \quad (10)$$

and use it to check the scaling of the system. Figure 2

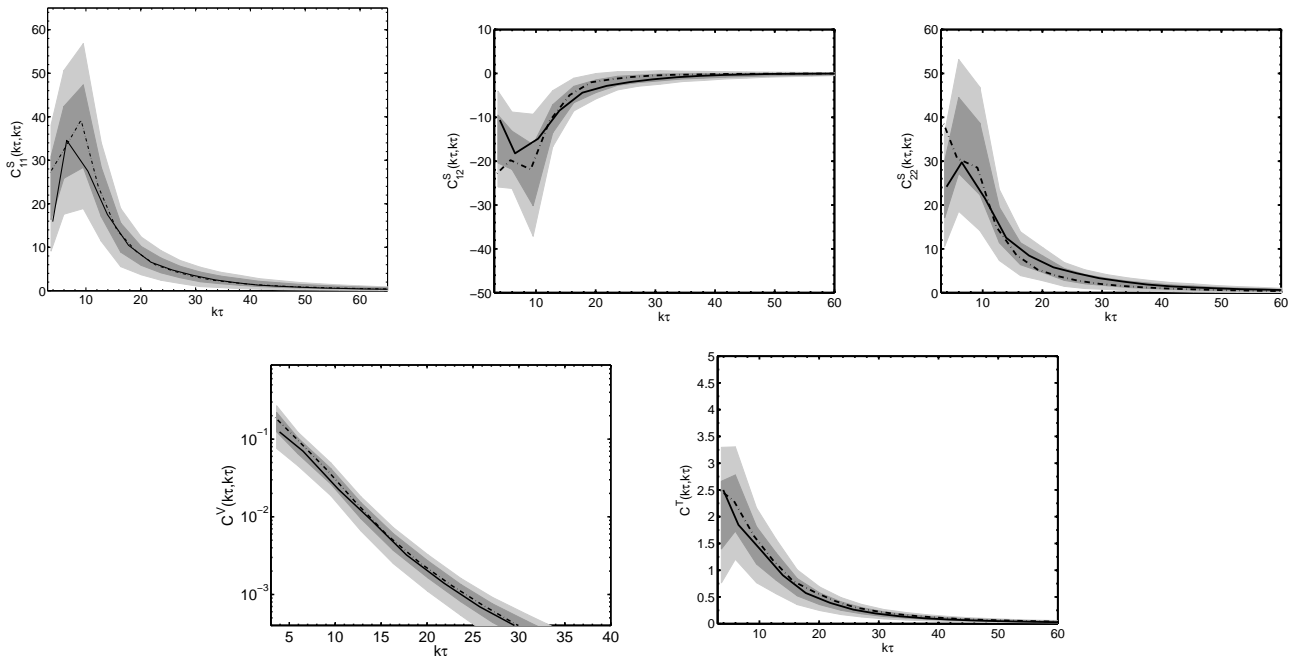


FIG. 3: The dependence of the 5 ETCs upon s in the radiation era at $\tau_{\text{sim}} = 128\eta^{-1}$. The shaded regions show the 1- σ and 2- σ uncertainties for the $s = 0.3$ case, while the lines indicate the $s = 1.0$ (solid), $s = 0.0$ (dot-dash) results, which clearly lie within the statistical uncertainties.

shows the result of the simulations for the radiation era for $s = 0.0, 0.3, 1.0$, as well as the best fit for times $\tau > 50$. First of all, note that the differences with respect to varying the value of s are minimal. It is also clear from these figures that after the initial non-scaling period, ξ follows a linear behaviour

$$\xi \propto (\tau - \tau_{\xi=0}). \quad (11)$$

There is nothing fundamental about the offset $\tau_{\xi=0}$, as argued for Abelian Higgs case in Ref. [37]; it is a consequence of the non-scaling initial period of the simulations and is negligible in the late-time limit of interest for CMB calculations. What is fundamental is the value of the slope of ξ , which shows little dependence upon s : 0.10 ± 0.01 for $s = 0.0$, 0.10 ± 0.02 for $s = 0.3$ and 0.09 ± 0.02 for $s = 1.0$. The difference between the three plots in Figure 2 is due almost entirely to differing values of $\tau_{\xi=0}$.

However, given that the system scales not with τ but with $\tau - \tau_{\xi=0}$, then following Ref. [37] we perform a rescaling of the measured UETC functions $\tilde{C}(k\tau, k\tau')$ in accordance with:

$$\tau \rightarrow \tau - \tau_{\xi=0}. \quad (12)$$

These functions then provide a more important test of scaling for the present work: after the rescaling, do they show negligible absolute time dependence? Figures 3 and 4 show the equal-time correlator (ETC) scaling functions, that is when $\tau = \tau'$. These are the most important part

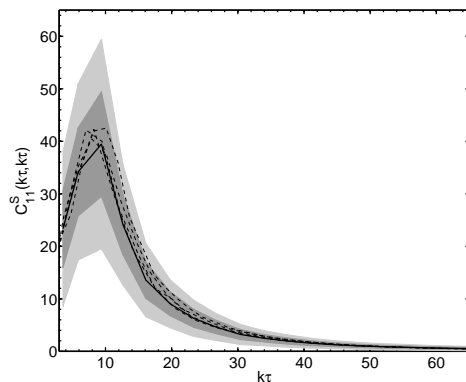


FIG. 4: The equal-time scaling function $\tilde{C}_{11}^S(k\tau, k\tau)$ averaged over five realizations for $s = 0.3$ in the radiation era. The different lines correspond to roughly uniformly spaced τ values in the range $50\eta^{-1} < \tau < 128\eta^{-1}$. The shaded regions show the 1- σ and 2- σ uncertainties in the mean indicated for the latest time (solid). For visualization purposes, the mean offset across the five realizations is used, whereas the actual CMB calculations use independent offsets for each realization.

of the UETCs, and the most suitable for visualization. The different lines in Fig. 4 correspond to the ETC function averaged over five realizations, for different times; the shaded regions correspond to the 1- σ and 2- σ uncertainties in the mean at the last time step (when the

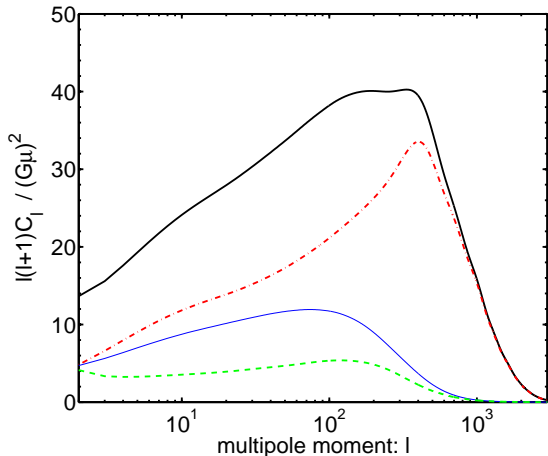


FIG. 5: CMB temperature power spectrum from semilocal string simulations. The solid black line is the total prediction, which is obtained by adding the contribution of scalar (dash-dot red), vector (thin blue) and tensor (dashed green) modes.

system is closest to scaling). Clearly, the different lines lie within the statistical uncertainties of the simulation, and there is no absolute dependence of the ETC on time. As the UETCs are the only quantities entering the CMB power spectrum calculations, we are confident that the earlier sampling does not affect the results.

We can also make use of the ETCs to show that the dependence of the simulations with s is quite mild. Figure 3 shows the ETCs for the last time step in the simulation for $s = 0.0, 0.3, 1.0$ for the five different UETCs need for the CMB calculation. In all cases the dependence on s lies well within the statistical uncertainties.

B. Temperature power spectra from semilocal strings

After checking that our numerical approach for simulating semilocal strings is satisfactory by monitoring the influence of the parameter s in the simulations and confirming the early onset of scaling, the resulting UETCs were fed into the modified CMBEASY Boltzmann code as explained in Section III. The perturbations obtained from the strings and from inflation are calculated separately and added in quadrature – the tiny interaction between the two contributions can be safely neglected. Besides, it is numerically quite slow to recompute the string spectra for many different values of the cosmological parameters. For these reasons, the string spectra were computed for a fixed value of the cosmological parameters

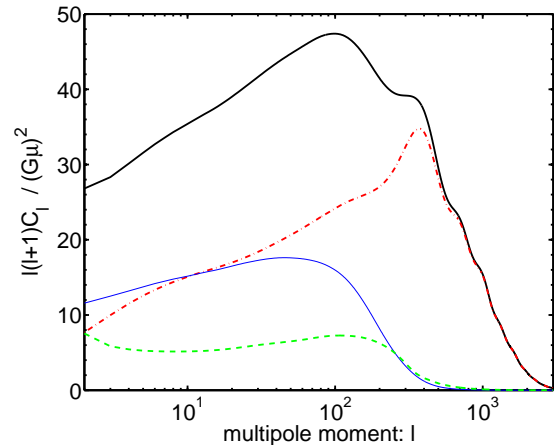
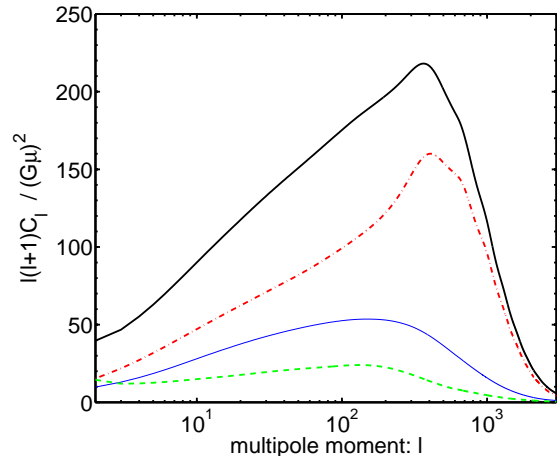


FIG. 6: CMB temperature power spectrum from Abelian Higgs strings (left) and texture (right) simulations. The solid black line is the total prediction, and its constituents: scalar (dash-dot red), vector (thin blue) and tensor (dashed green). Note the difference in the scale between the two graphs.

(the central values given by cosmological experiments²). We then tested at the end that the string spectra do not change significantly when the cosmological parameters are varied within the limits imposed by the CMB data. Note that this is the only point where the cosmological parameters are involved in the calculation of the CMB spectra.

Figure 5 shows the CMB temperature power spectrum from semilocal cosmic strings, divided into scalar, vector and tensor components. For comparison, we plot the corresponding power spectra from Abelian Higgs strings and textures in Fig. 6. The power spectra for Abelian Higgs

² The calculation of the string spectra was done for $h=0.72$ [62], $\Omega_b h^2 = 0.0214$ [63], $\Omega_\Lambda = 0.75$ [64]. We also assumed spatial flatness and the optical depth to the last-scattering surface $\tau = 0.1$.

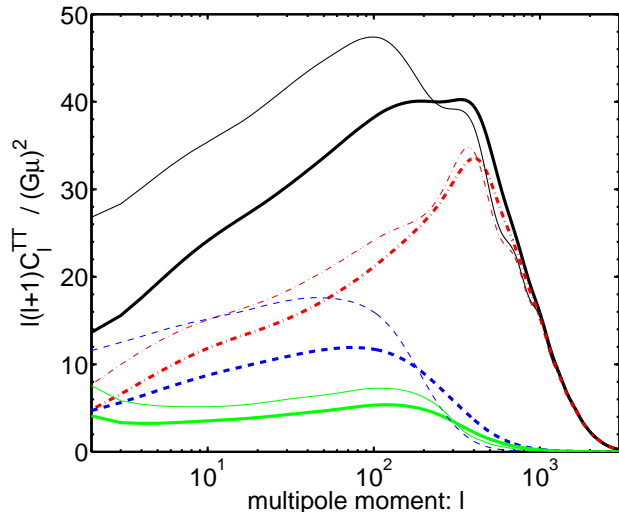


FIG. 7: The temperature power spectra from semilocal strings (thick) and textures (thin), showing the scalar (dash-dot red), vector (dashed blue) and tensor (lower solid green) components.

strings are taken from Ref. [37],³ whereas the texture spectra have been calculated by using new simulations of the texture linear- σ model obtained by setting to zero the gauge fields in the semilocal model Eq. (1) (see Appendix for details on the texture calculations).

The first thing to notice from these graphs is that, at fixed $G\mu$, the Abelian Higgs strings give significantly higher anisotropies than the other two by a factor of about 5. Semilocal strings and textures are quite similar, with the former being slightly lower. This is in good accord with the intuition that semilocal strings ought to be similar to textures, but with some of the anisotropies cancelled by the gauge field. Ultimately, this difference in anisotropy amplitude will result in a weakening of observational constraints on $G\mu$ for semilocal and texture as compared to Abelian Higgs strings.

Going beyond the amplitude, it is clear that the semilocal temperature power spectra shape shares properties with both the Abelian Higgs and the texture prediction. It is close to the texture prediction in, e.g., the level of the power of the anisotropies at fixed $G\mu$, although it does not have the small oscillations. On the other hand, it peaks for larger values of ℓ than textures, more like Abelian Higgs strings.

Figure 7 shows a direct comparison between the semilo-

³ Refs. [15, 37] employed a code in which a bug has been discovered, and this had a small effect in Ref. [13] since it used their results directly (see the respective errata). Here we have used the corrected power spectra from Refs. [15, 37] and quote the corrected results from Ref. [13].

	$G\mu_{10}$
Abelian Higgs string	2.7×10^{-6}
Semilocal string	5.3×10^{-6}
Textures	4.5×10^{-6}

TABLE II: Normalization of different defects to match the observed $\ell = 10$ multipole value.

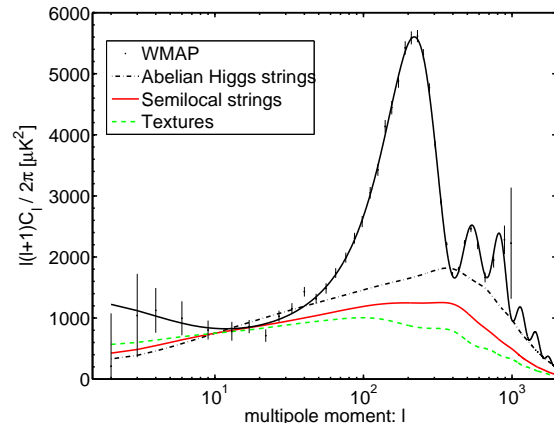


FIG. 8: The temperature power spectra for Abelian Higgs strings, semilocal strings, textures and the best fit inflationary model. The points represent the three-year WMAP experimental data [65]. The curves for defects are normalized to match the data at $\ell = 10$.

cal strings prediction and the texture prediction for the temperature power spectrum. As discussed before, the texture model can be obtained by setting to zero the gauge coupling constant in the semilocal model, so the differences appearing in the curves arise from coupling the scalar fields to the gauge fields. The overall shape of the curves for each model is roughly the same, with that for textures being somewhat higher and peaking earlier than that for the semilocal strings. If the Abelian Higgs model prediction was plotted in the same graph, it would lie way above this curve, since the overall scale of the spectrum is much higher.

However, bear in mind that the normalization of the spectra is a free parameter, and one would like to compare the relative shapes of the predictions to understand their detailed observational implications. For example, it is customary to encode the information about the overall power coming from the defects by $G\mu_{10}$. The normalization of the strings is proportional to $(G\mu)^2$. Thus, $G\mu_{10}$ is the value of the normalization by which the defect spectra matches the WMAP data [65] at multipole $\ell = 10$, shown in Table II for each type of defect. This is merely a tool to compare different predictions. Figure 8 shows pictorially the different defect predictions with these normalizations, together with the experimental data and the inflationary best-fit model. Note that for textures it is not natural to talk about “energy per

unit length”, but we adopt the same normalization strategy Eq. (2) by analogy with the strings, in order to ease the comparison between models. Different normalization schemes are discussed in the Appendix.

C. Polarization power spectra from semilocal strings

The polarization power spectra are shown in Fig. 9, decomposed as usual into the EE, TE and BB components [66]. The curves are normalized so they have equal TT power at $\ell = 10$ (and match the WMAP measurement on this scale).⁴ Note that, as in Ref. [15], we do not include the coupling between inflation and defect perturbations as a result of gravitational lensing at late times. We do not, however, expect this effect to be significant: the gravitational lensing of the inflationary scalar EE spectrum by the defect perturbations is likely to be insignificant relative to that produced by the inflationary perturbations, since defects are sub-dominant. It is also likely to be negligible relative to the B-mode from defects since defects still produce a strong B-mode signal even when their sub-dominance is taken into account. The lensing of the defect EE and BB spectra by the inflationary perturbations should be negligible also since defects contribute equally strongly to these two spectra.

With the temperature spectra all normalized to the same value at $\ell = 10$, the polarization spectra are all of similar magnitude and shape (if normalized to the same $G\mu$, the Abelian Higgs contribution would be much higher). In the EE case, all three defect models peak at the same value of $\ell \sim 1000$, with the semilocal component having slightly less pronounced oscillations, and the secondary peak at low ℓ coming from reionization follows the following trend: it peaks at the lowest value of ℓ for textures, next for semilocal strings, and highest for Abelian Higgs strings. The same trend can be seen for the low- ℓ features of the TE spectra. The high- ℓ behaviour of the TE is roughly the same for all three cases, showing large oscillations that eventually die out. Note, however, that the oscillations for the semilocal case are the smallest, and there is no alternation between anticorrelation and correlation due to the combined effect of the scalar–vector–tensor contributions which have different phases.

The BB power spectrum is arguably the most interesting prediction from defects [14, 15, 18, 35]: inflation contributes weakly to the BB polarization [67], and the signal predicted from defects might be detected in the near future, providing a smoking gun for the existence of defects in cosmology. In Fig. 9 it can be seen that

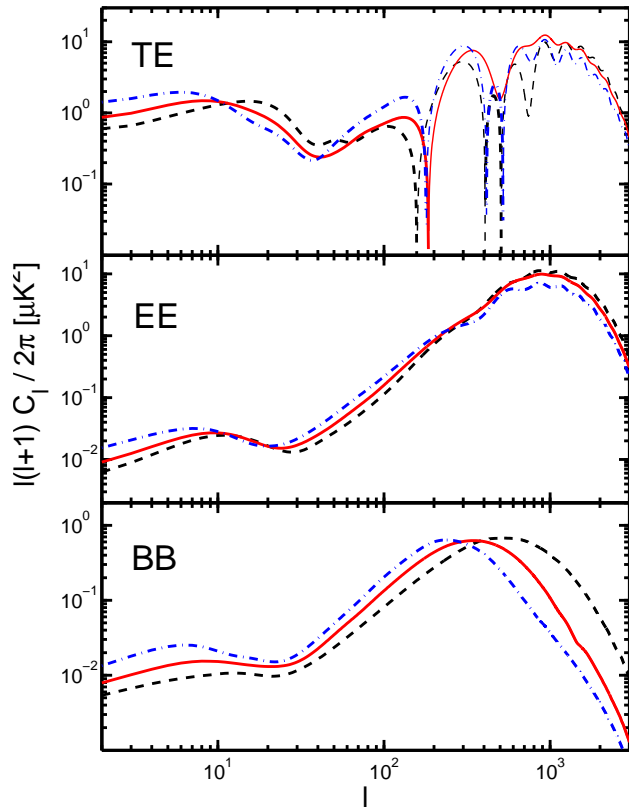


FIG. 9: Polarization power spectra for semilocal strings (solid red), compared to Abelian Higgs strings (dashed black) and textures (dot-dash blue). The top figure is the TE power spectra, the EE is in the middle, and BB at the bottom. All the curves are normalized by making the temperature spectra match the WMAP $\ell = 10$ value, i.e., using the values of $G\mu = G\mu_{10}$ as in table II. In the TE figure, the thick lines correspond to correlations and the thin lines to anticorrelations. The results plotted here correspond to a value $\tau = 0.1$ (see footnote 2).

the shape of the BB power spectra is similar for semilocal strings, textures and Abelian Higgs string. Both peaks follow the aforementioned trend, with textures peaking for lowest $\ell \sim 240$, then semilocal strings $\ell \sim 360$, and finally Abelian Higgs strings $\ell \sim 590$; furthermore, the BB power spectrum for textures decays first, then that for semilocal strings, and the Abelian Higgs string BB power spectrum decays at the highest ℓ .

V. CONSTRAINTS FROM CURRENT CMB DATA

Clearly, a string component at the $G\mu_{10}$ level shown in Table II is ruled out by the experiments. There-

⁴ See Fig. 12 in Section V for a figure with the normalization of each case set to match the respective 95% upper limits from current data.

Parameter	PL	PL+SL	PL+AH	PL+TX
f_{10}	0	0.14 ± 0.06	0.09 ± 0.05	0.18 ± 0.08
n_s	0.96 ± 0.02	1.02 ± 0.04	1.00 ± 0.03	1.04 ± 0.05
h	0.74 ± 0.03	0.85 ± 0.06	0.84 ± 0.06	0.87 ± 0.08
$\Omega_b h^2$	0.0223 ± 0.0007	0.0263 ± 0.0021	0.0258 ± 0.0020	0.0264 ± 0.0026
$\Omega_m h^2$	0.126 ± 0.007	0.122 ± 0.007	0.122 ± 0.007	0.118 ± 0.008
$\ln(10^{10} A_s^2)$	3.09 ± 0.06	2.96 ± 0.08	2.99 ± 0.08	2.94 ± 0.09
τ	0.09 ± 0.03	0.11 ± 0.04	0.11 ± 0.04	0.12 ± 0.04

TABLE III: Mean and standard deviations of the power-law model parameters, using CMB data only.

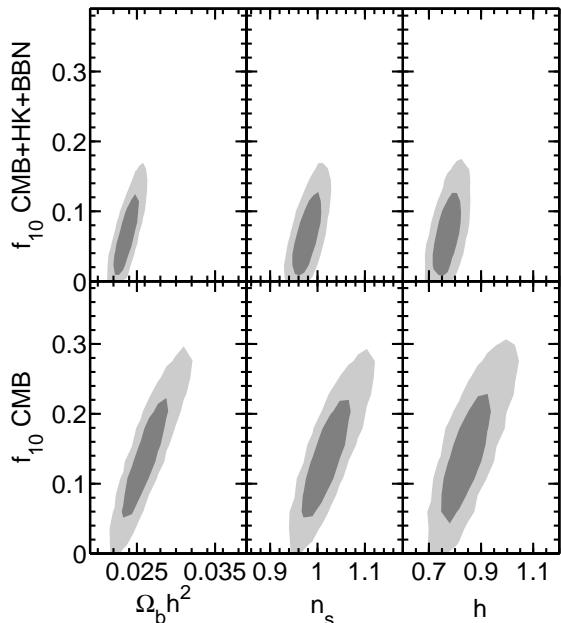
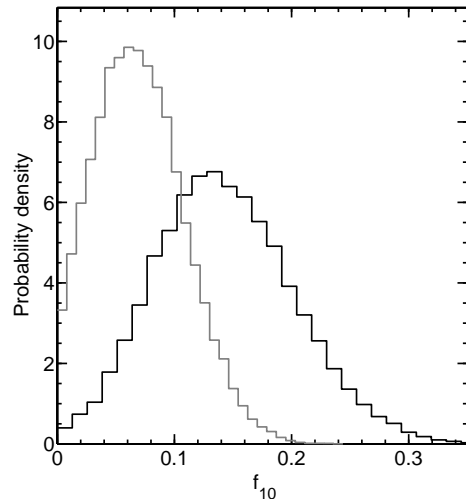


FIG. 10: The 2-dimensional constraints from the MCMC chains using CMB only data (bottom), and using CMB+BBN+HKP data (top).

fore, in order to quantify the allowed level for a string component, we introduce a parameter f_{10} [13]: the fractional contribution of strings to the temperature power spectra at multipole $\ell = 10$. We then use a modified version of CosmoMC [68] to perform a multi-parameter Markov Chain Monte Carlo (MCMC) likelihood analysis for CMB data (WMAP, ACBAR, BOOMERANG, CBI and VSA projects [65, 69, 70, 71, 72, 73]) when semilocal strings or textures are included. We also reproduce the results for Abelian Higgs strings from [13] for comparison. The likelihood analysis is performed for the usual six-parameter Power-Law (PL) model ($\Omega_b h^2$, h , n_s , τ , $\Omega_m h^2$, A_s), plus the new extra f_{10} . We vary only the normalization of the string (or texture) power spectra and keep the form of them fixed, following Refs. [9, 13]. This approach is justified since the strings (or textures) contribute only a small fraction to the total power, and the changes in the cosmological parameters are not large

FIG. 11: The 1-dimensional marginalized likelihood plots for the fraction of semilocal strings f_{10} allowed at multipole $\ell = 10$ from the MCMC chains using CMB only data (dark), and using CMB+BBN+HKP data (light).

enough that the changes in the form of the string or texture spectra are relevant. The best-fit values of the parameters can be found in Table III for PL alone, and for PL with semilocal (SL) strings, Abelian Higgs (AH) strings and textures (TX).

Table III shows that, as in previous results [9, 13], the degeneracies of the cosmological parameters with respect to the CMB data allow for a rather high value of $f_{10} = 0.14 \pm 0.06$, which corresponds to $G\mu = [1.9 \pm 0.4] \times 10^{-6}$. In order to accommodate the defect contribution, other parameters (most notably $\Omega_b h^2$, h , and n_s) get shifted to higher values, as was the case for the Abelian Higgs strings [13].

Figure 10 shows the marginalized 2D likelihood distributions for the parameters $\Omega_b h^2$, h , and n_s versus f_{10} . It is clear in the figure that there is ample space for a noticeable value of f_{10} . In fact, it can be seen in the 1-D marginalized likelihood plot (Fig. 11) that the CMB data alone prefers to have semilocal strings at a 2- σ level.

However, as mentioned before (see Table III), the best-fit values of $\Omega_b h^2$ and h are high compared to the con-

cordance model: Non-CMB experiments for those two quantities yield $h = 0.72 \pm 0.8$ (the Hubble Key Project HKP [62]) and $\Omega_b h^2 = 0.0214 \pm 0.0020$ (measurements of deuterium abundance in high-redshift gas clouds together with big bang nucleosynthesis BBN [63]). If we include these two non-CMB experimental values into our MCMC scheme (as gaussian likelihoods), we confirm that the new set of data is more constraining also for semilocal strings (as seen in Figs. 10 and 11). However, the 95% confidence level upper bound on f_{10} for semilocal strings remains rather high, going from $G\mu < 2.6 \times 10^{-6}$ ($f_{10} < 0.25$) for the CMB only case to $G\mu < 2.0 \times 10^{-6}$ ($f_{10} < 0.14$).

We may now use these upper bounds to compare the strengths of the power spectra of different models. Table IV summarises the values of f_{10} and $G\mu$ we obtain for our analysis of semilocal strings and textures, together with that for Abelian Higgs strings from Ref. [13]. The parameter f_{10} depends mainly on the form of the defect power spectra, and we see that the data allow for a higher contribution from semilocal strings (and textures) than from Abelian Higgs strings. Besides, the values of $G\mu_{10}$ are also higher for semilocal strings (and textures) than for the Abelian Higgs strings. Therefore, the expectation that the constraints on the Abelian Higgs string tensions would be alleviated by semilocal strings is confirmed: the 95% upper bound limit for semilocal strings is $G\mu < 2.0 \times 10^{-6}$ for CMB+BBN+HKP ($G\mu < 2.6 \times 10^{-6}$ for CMB only) whereas for Abelian Higgs string it is $G\mu < 0.9 \times 10^{-6}$ for CMB+BBN+HKP ($G\mu < 1.1 \times 10^{-6}$ for CMB only).

Figure 12 shows the temperature power spectrum and the BB polarization spectrum for semilocal strings, Abelian Higgs strings and textures, normalized by using the upper bounds obtained from performing the MCMC likelihood analysis for both CMB and non-CMB (BBN and HKP) data. In the temperature power spectrum figure it can be seen that due to the different shapes of the curves, even though the textures are allowed the highest level of power at $\ell = 10$, the semilocal and Abelian Higgs strings go up to higher peaks. The signal is highest for textures for $\ell \lesssim 60$, for semilocal strings for $60 \lesssim \ell \lesssim 250$ and then for Abelian Higgs for $250 \lesssim \ell$. On the other hand, for the BB polarization, the normalization makes the trend of the power coming from the three cases just the reverse of the temperature case: textures have the highest peak, followed by semilocal strings and then Abelian Higgs strings. Needless to say, the normalization does not change the value of ℓ at which each case peaks, and we find that textures peak first, then semilocal strings, and then Abelian Higgs strings.

It is worth mentioning that, in all cases studied, the value for the spectral index n_s is higher than the one obtained for cases without defects; and $n_s = 1$ is not ruled

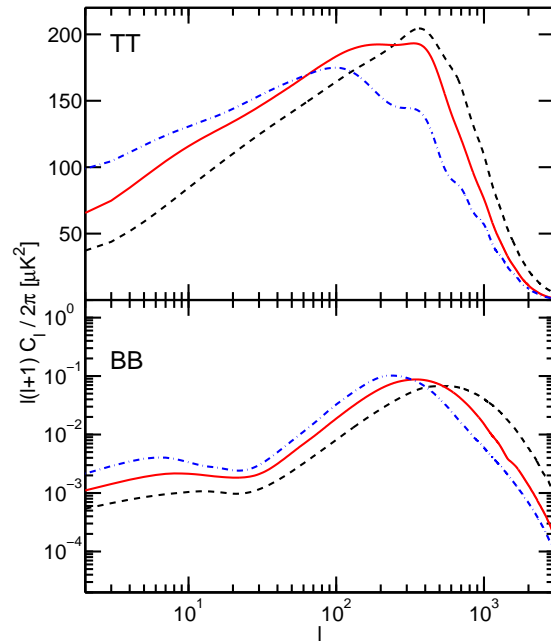


FIG. 12: Temperature power spectra (top) and BB polarization power spectra (bottom) for semilocal strings (solid red), compared to Abelian Higgs strings (dashed black) and textures (dot-dash blue). The curves are normalized using the 95% confidence level upper bound from a MCMC analysis using CMB, BBN and HKP data.

Model	CMB only			CMB+BBN+HKP		
	f_{10}	$G\mu$	n_s	f_{10}	$G\mu$	n_s
SL	0.25	2.6×10^{-6}	1.09	0.14	2.0×10^{-6}	1.01
TX	0.33	2.5×10^{-6}	1.14	0.16	1.8×10^{-6}	1.02
AH	0.17	1.1×10^{-6}	1.06	0.10	0.9×10^{-6}	1.00

TABLE IV: 95% upper bounds on f_{10} , $G\mu$ and n_s for PL+X, using CMB only, and using CMB+BBN+HKP.

out⁵ (see table IV). Therefore, when comparing different cosmological models, one should also consider the (scale-invariant) Harrison–Zel’dovich (HZ) model with 5 parameters ($\Omega_b h^2$, h , τ , $\Omega_m h^2$, A_s) and a fixed $n_s = 1$.

Table V shows the goodness of fit for the concordance PL model, as well as for the HZ model, when Abelian Higgs strings, semilocal strings and textures are added; for both CMB only and CMB+BBN+HKP data. In most cases, the inclusion of the defects makes the fit better, with semilocal strings obtaining marginally the best fit. This is not too surprising for the cases where defects

⁵ See Ref. [74] for a discussion about n_s in light of WMAP3 from a Bayesian model selection point of view.

Model	CMB only		CMB+BBN+HKP	
	$\Delta\chi^2$	$\ln(E)$	$\Delta\chi^2$	$\ln(E)$
HZ	6.6	-0.6 ± 0.1	8.4	-1.4 ± 0.1
PL	0	0	0	0
HZ+SL	-4.4	2.5 ± 0.2	-0.7	1.0 ± 0.3
PL+SL	-4.5	1.0 ± 0.3	-1.9	-1.0 ± 0.1
HZ+AH	-3.5	1.8 ± 0.2	1.4	-0.7 ± 0.2
PL+AH	-3.5	-0.1 ± 0.2	-1.4	-1.8 ± 0.2
HZ+TX	-3.2	2.0 ± 0.3	-0.5	0.3 ± 0.3
PL+TX	-3.4	1.2 ± 0.3	-1.2	-1.2 ± 0.1

TABLE V: Goodness of fit and Bayesian Evidence relative to the concordance model PL.

are added to the PL model, because we are adding an extra parameter to the PL model, and of course obtaining a better fit. But the models with HZ + defects have the same number of parameters as the PL model (6 parameters), and surprisingly, the fit is better when considering CMB data only.

In order to compare different models, we use Bayesian evidence values [75]. The evidences are calculated using the Savage–Dickey method [76, 77] with flat priors of $0 < f_{10} < 1$ and $0.75 < n_s < 1.25$ (Table V). In the case of CMB data only, adding a defect contribution to the PL model makes little change to the evidence, whereas HZ+defects models have a significant higher evidence (and semilocal strings are marginally better than textures or Abelian Higgs strings). Therefore, taken at face value, HZ+SL strings is the six-parameter model which fits the data best, though the others are not convincingly worse. With the non-CMB data added, the evidences get reduced, but not to the level to conclude that a string contribution is ruled out.

This type of comparison will have some dependence on the choice of prior used for the defect component (the other priors are less important as they are shared by the models). Our imposition of a prior on f_{10} is just one out of several plausible options. A prior on μ might be more appropriate but is hard to formulate; for instance a logarithmic (Jeffreys) prior on μ would put most of the prior weight on models with negligible defect contribution and hence leave the data unable to distinguish them (the same situation occurs with the inflationary tensor component – see Ref. [74]). In any event, we can safely say that present data are not good enough to exclude a defect contribution, and leave open the tantalising possibility that such a contribution may be a significant one.

VI. DISCUSSION

In this article we report on the first ever semilocal string simulations to predict CMB power spectra. This has been possible because of recent improvements in simulating field theoretical defects, as there is no Nambu–Goto type approximation for semilocal strings. The case

of Abelian Higgs model strings is much better known, so we compared the semilocal string predictions to the Abelian Higgs string ones, trying to minimize the differences in the approaches. Since semilocal strings were expected to share properties with both an Abelian Higgs string prediction and a texture prediction, we also produced a set of simulations for texture-type defects to compare all three defect contributions.

Our first conclusion is that the amplitude of the spectra for the semilocal strings is indeed lower than in Abelian Higgs models (for a given energy scale); therefore, the normalization at $\ell = 10$ to match the WMAP value gives a higher value for semilocal strings $G\mu_{10} = 5.3 \times 10^{-6}$ than for Abelian Higgs strings $G\mu_{10} = 2.7 \times 10^{-6}$. Moreover, the form of the power spectra for semilocal strings allows for their fractional contribution to the temperature power spectra at multipole $\ell = 10$ to be higher than the one for Abelian Higgs strings: the 95% confidence upper bounds are $f_{10} < 0.25$ ($f_{10} < 0.14$) for semilocal strings for CMB only (CMB+BBN+HKP); whereas $f_{10} < 0.17$ ($f_{10} < 0.10$) for Abelian Higgs strings.

These two ingredients contribute to allow a higher value of $G\mu$ for semilocal strings when CMB data (and also when HKP and BBN data) are taking into account: $G\mu < 2.6 \times 10^{-6}$ ($G\mu < 2.0 \times 10^{-6}$) for semilocal strings for CMB only (CMB+BBN+HKP); whereas $G\mu < 1.1 \times 10^{-6}$ ($G\mu < 0.9 \times 10^{-6}$) for Abelian Higgs strings. Thus, if a promising high-energy physics inflation model faces a problem of creating Abelian Higgs cosmic strings at a scale that it is too high for the CMB, a possible resolution could be to extend the model to predict semilocal strings instead. This weakens the $G\mu$ constraint by a factor of nearly three, which may give the theory extra breathing space.

As in the case of textures [9] and local strings [11, 13], the best fit for the cosmological parameters when taking into account semilocal strings gives a rather high spectral index n_s , comparing to the concordance model. For CMB only data, the preferred value of n_s is higher than 1 ($n_s = 1.02 \pm 0.04$), whereas if BBN and HKP data are included $n_s = 0.98 \pm 0.02$. This is in contrast to the Abelian Higgs data, where the CMB data alone predict $n_s = 1$; but the result is very similar when BBN and HKP data are included [13]. This result also alleviates pressure on high-energy physics models (such as D-term and F-term hybrid inflation) which predict defects and an n_s close to unity.

As $n_s = 1$ is close to our best-fit values, we studied how well a combination of Harrison–Zel’dovich plus defects would fit the data, comparing it to the concordance model. Using goodness of fit and Bayesian Evidence criteria, we find that models with defects are not ruled out (even when BBN and HKP data are included), and should be considered as competitive models. In fact, taking into account only CMB data, there is significant evidence in favour of a Harrison–Zel’dovich plus semilocal strings model.

We have not included large-scale structure datasets

into our analysis for two reasons. Firstly, perturbations from defects are non-linear and non-Gaussian as soon as they are created [9], and so it is not clear that the commonly-used model [78] for non-linear corrections to the galaxy power spectrum applies. Secondly, recent analyses [79, 80] show scale-dependent bias even on relatively large scales ($0.05 < k/h\text{Mpc}^{-1} < 0.15$), and make clear that more work is needed before the galaxy power spectrum can be used for robust estimates of cosmological parameters.

The prediction for polarization power spectra from semilocal strings is similar to that of Abelian Higgs strings. As a matter of fact, the height of the BB polarization peak (normalized using the 95% confidence level upper bound on f_{10}) is of the same order of magnitude for Abelian Higgs strings, semilocal strings and textures, though the position at which the maximum occurs vary from case to case. A detection of a BB signal on these scales could be an indicator of the existence of cosmic defects [15].

In the present work we have studied only BPS semilocal strings, but we will in a future work extend the analysis to lower values of β , which would arise in F-term supersymmetric models (or even in P-term models [81, 82]). The behaviour of semilocal strings does depend strongly of β [40]: the lower the value of β the more the semilocal strings behave as Abelian Higgs strings. Tracking how the CMB predictions change with respect to β will give us insight into how the different components in a string network contribute to the creation of anisotropies.

There is also a whole new class of strings coming from string inflation: (p, q) -strings [6, 7, 8]. Even though there is some work about the networks of these defects [83, 84, 85, 86], basic properties, such as scaling, are still not really understood. Provided some sound CMB predictions from these strings are calculated, it would be interesting to compare the results with those of Abelian Higgs or semilocal strings.

Ultimately, one would like to be able to discriminate between all the different defect types, be it Abelian Higgs, semilocal, textures or (p, q) -strings. As we have shown here, the predictions do look similar, but there are differences, e.g., the aforementioned position of the BB peak. The question is whether these differences are strong enough, or whether future data will be good enough, to pinpoint whether defects do appear and if so, which type. In a future publication we will address this issue.

Acknowledgments

We thank M. Nitta for pointing out Ref. [49] and K. Sousa for discussion. We acknowledge support from PPARC/STFC (N.B., M.H, A.R.L.), the Swiss NSF (M.K.), Marie Curie Intra-European Fellowship MEIF-CT-2005-009628 (J.U.). This work was partially supported by Basque Government (IT-357-07), the Spanish Consolider-Ingenio 2010 Programme CPAN (CSD2007-

00042) and FPA2005-04823 (J.U.). The simulations were performed on COSMOS, the UK National Cosmology Supercomputer, supported by SGI, Intel, HEFCE and PPARC.

APPENDIX A: TEXTURE SIMULATIONS

In this work we have compared the CMB predictions to those from the Abelian Higgs model and texture models. For the latter we have performed a new set of simulations for the linear- σ global texture model comparing the results additionally with previous ones from Refs. [9, 35, 36, 87].

We exploited the fact that a texture model can be obtained directly from Lagrangian Eq. (1) by setting the gauge field to zero, obtaining

$$\begin{aligned} \mathcal{L} &= |\partial_\mu \phi_1|^2 + |\partial_\mu \phi_2|^2 - \frac{\lambda}{4} \left(|\phi_1|^2 + |\phi_2|^2 - \eta^2 \right)^2 \\ &= \sum_{i=1}^4 (\partial_\mu \psi_i)^2 - \frac{\lambda}{4} \left(\sum_{i=1}^4 \psi_i^2 - \eta^2 \right)^2 \end{aligned} \quad (\text{A1})$$

where ψ_i , ($i = 1...4$) are real scalar fields and $\phi_1 = \psi_1 + i\psi_2$, $\phi_2 = \psi_3 + i\psi_4$.

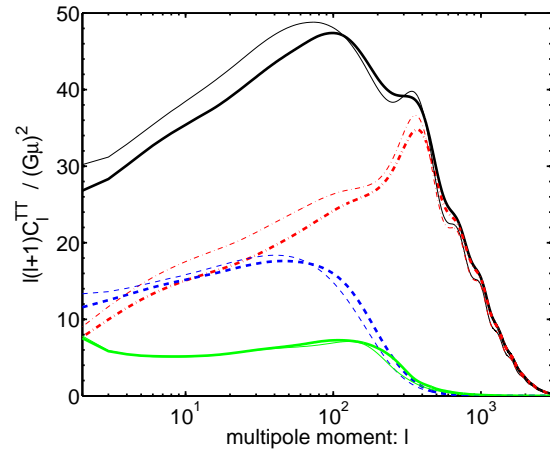


FIG. 13: The temperature power spectra from linear σ textures (thick) obtained and used in this article; together with the spectra from a non-linear σ model (thin) from [37]. The different components are scalar (dash-dot red), vector (dashed blue) and tensor (lower solid green).

This is the Lagrangian we have simulated to obtain the figures used in the main body of this article. Note that it is not canonically normalized with respect to the real scalar fields, which becomes clear when compared to the non-linear σ model:

$$\mathcal{L} = \frac{1}{2} \sum_{i=1}^4 (\partial_\mu \tilde{\psi}_i)^2 - \tilde{\lambda} \left(\sum_{i=1}^4 \tilde{\psi}_i^2 - \kappa^2 \right) \quad (\text{A2})$$

where in this case $\tilde{\lambda}$ is a Lagrange multiplier fixing the fields onto the vacuum manifold.

The normalization of the textures is usually given for the Lagrangian canonically normalized for scalar fields as [53]

$$\varepsilon = 4\pi G\kappa^2. \quad (\text{A3})$$

Comparing both Lagrangians (A1) and (A2), it can be seen that $\kappa^2 = 2\eta^2$, so the normalization scheme for textures used throughout this work Eq. (2) relates to that of Ref. [53] by

$$\varepsilon = 4G\mu \quad (\text{A4})$$

Note that Ref. [35] uses another definition of ε , bigger by a factor 2π .

The procedure followed to obtain the CMB predictions from textures was exactly the same as for the semilocal case (and for the Abelian Higgs case). The results can be seen in Fig. 6. Earlier work on global textures [41, 88, 89] represented important steps towards the formalism we are using here. However, they neglected decoherence and so overemphasized the presence of the acoustic peaks.

We also compared the texture predictions we obtain in our simulations with those of a non-linear σ model by some of the authors of this article [37] in Fig. 13. Those simulations were performed using different parameters; e.g., smaller lattices (256^3) and smaller number of eigenvectors used to obtain the CMB power spectra. In any case, the agreement with our linear- σ model is very good, which makes our comparison of texture with semilocal and Abelian Higgs strings more widely valid.

-
- [1] A. Vilenkin and E. P. S. Shellard, *Cosmic Strings and Other Topological Defects* (Cambridge University Press, Cambridge, U.K., 1994).
- [2] M. B. Hindmarsh and T. W. B. Kibble, Rept. Prog. Phys. **58**, 477 (1995), hep-ph/9411342.
- [3] D. H. Lyth and A. Riotto, Phys. Rept. **314**, 1 (1999), hep-ph/9807278.
- [4] R. Jeannerot, J. Rocher, and M. Sakellariadou, Phys. Rev. **D68**, 103514 (2003), hep-ph/0308134.
- [5] M. Majumdar and A. Christine-Davis, JHEP **03**, 056 (2002), hep-th/0202148.
- [6] S. Sarangi and S. H. H. Tye, Phys. Lett. **B536**, 185 (2002), hep-th/0204074.
- [7] E. J. Copeland, R. C. Myers, and J. Polchinski, JHEP **06**, 013 (2004), hep-th/0312067.
- [8] G. Dvali and A. Vilenkin, JCAP **0403**, 010 (2004), hep-th/0312007.
- [9] N. Bevis, M. Hindmarsh, and M. Kunz, Phys. Rev. **D70**, 043508 (2004), astro-ph/0403029.
- [10] M. Wyman, L. Pogosian, and I. Wasserman, Phys. Rev. **D72**, 023513 (2005), astro-ph/0503364 [Erratum-ibid. **D73** (2006) 089905].
- [11] R. A. Battye, B. Garbrecht, and A. Moss, JCAP **0609**, 007 (2006), astro-ph/0607339.
- [12] A. A. Fraisse, JCAP **0703**, 008 (2007), astro-ph/0603589.
- [13] N. Bevis, M. Hindmarsh, M. Kunz, and J. Urrestilla, Phys. Rev. Lett. **100**, 021301 (2008), astro-ph/0702223 [Erratum in preparation].
- [14] U. Seljak and A. Slosar, Phys. Rev. **D74**, 063523 (2006), astro-ph/0604143.
- [15] N. Bevis, M. Hindmarsh, M. Kunz, and J. Urrestilla, Phys. Rev. **D76**, 043005 (2007), arXiv:0704.3800 [astro-ph] [Erratum in preparation].
- [16] R. A. Battye, B. Garbrecht, A. Moss, and H. Stoica, JCAP **0801**, 020 (2008), 0710.1541.
- [17] A. A. Fraisse, C. Ringeval, D. N. Spergel, and F. R. Bouchet (2007), arXiv:0708.1162 [astro-ph].
- [18] L. Pogosian and M. Wyman (2007), arXiv:0711.0747 [astro-ph].
- [19] J. Urrestilla, A. Achucarro, and A. C. Davis, Phys. Rev. Lett. **92**, 251302 (2004), hep-th/0402032.
- [20] K. Dasgupta, J. P. Hsu, R. Kallosh, A. Linde, and M. Zagermann, JHEP **08**, 030 (2004), hep-th/0405247.
- [21] A. Achucarro, A. Celi, M. Esole, J. Van den Bergh, and A. Van Proeyen, JHEP **01**, 102 (2006), hep-th/0511001.
- [22] K. Dasgupta, H. Firouzjahi, and R. Gwyn, JHEP **04**, 093 (2007), hep-th/0702193.
- [23] T. Vachaspati and A. Achucarro, Phys. Rev. **D44**, 3067 (1991).
- [24] B. Allen, R. R. Caldwell, E. P. S. Shellard, A. Stebbins, and S. Veeraraghavan, Phys. Rev. Lett. **77**, 3061 (1996), astro-ph/9609038.
- [25] B. Allen, R. R. Caldwell, S. Dodelson, L. Knox, E. P. S. Shellard, and A. Stebbins, Phys. Rev. Lett. **79**, 2624 (1997), astro-ph/9704160.
- [26] C. Contaldi, M. Hindmarsh, and J. Magueijo, Phys. Rev. Lett. **82**, 679 (1999), astro-ph/9808201.
- [27] M. Landriau and E. P. S. Shellard, Phys. Rev. **D69**, 023003 (2004), astro-ph/0302166.
- [28] G. R. Vincent, M. Hindmarsh, and M. Sakellariadou, Phys. Rev. **D56**, 637 (1997), astro-ph/9612135.
- [29] V. Vanchurin, K. D. Olum, and A. Vilenkin, Phys. Rev. **D74**, 063527 (2006), gr-qc/0511159.
- [30] V. Vanchurin, K. Olum, and A. Vilenkin, Phys. Rev. **D72**, 063514 (2005), gr-qc/0501040.
- [31] C. Ringeval, M. Sakellariadou, and F. Bouchet, JCAP **0702**, 023 (2007), astro-ph/0511646.
- [32] C. J. A. P. Martins and E. P. S. Shellard, Phys. Rev. **D73**, 043515 (2006), astro-ph/0511792.
- [33] A. Albrecht, R. A. Battye, and J. Robinson, Phys. Rev. Lett. **79**, 4736 (1997), astro-ph/9707129.
- [34] L. Pogosian and T. Vachaspati, Phys. Rev. **D60**, 083504 (1999), astro-ph/9903361.
- [35] U.-L. Pen, U. Seljak, and N. Turok, Phys. Rev. Lett. **79**, 1611 (1997), astro-ph/9704165.
- [36] R. Durrer, M. Kunz, and A. Melchiorri, Phys. Rev. **D59**, 123005 (1999), astro-ph/9811174.
- [37] N. Bevis, M. Hindmarsh, M. Kunz, and J. Urrestilla, Phys. Rev. **D75**, 065015 (2007), astro-ph/0605018 [Erratum in preparation].
- [38] A. Achucarro, J. Borrill, and A. R. Liddle, Phys. Rev.

- D57**, 3742 (1998), hep-ph/9702368.
- [39] A. Achucarro, J. Borrill, and A. R. Liddle, Phys. Rev. Lett. **82**, 3742 (1999), hep-ph/9802306.
- [40] A. Achucarro, P. Salmi, and J. Urrestilla, Phys. Rev. **D75**, 121703 (2007), astro-ph/0512487.
- [41] R. Durrer and Z. H. Zhou, Phys. Rev. **D53**, 5394 (1996), astro-ph/9508016.
- [42] A. Achucarro, A. C. Davis, M. Pickles, and J. Urrestilla, Phys. Rev. **D66**, 105013 (2002), hep-th/0109097.
- [43] M. Pickles and J. Urrestilla, JHEP **01**, 052 (2003), hep-th/0211240.
- [44] A. Achucarro and T. Vachaspati, Phys. Rept. **327**, 347 (2000), hep-ph/9904229.
- [45] M. Hindmarsh, Phys. Rev. Lett. **68**, 1263 (1992).
- [46] M. Hindmarsh, Nucl. Phys. **B392**, 461 (1993), hep-ph/9206229.
- [47] R. A. Leese and T. M. Samols, Nucl. Phys. **B396**, 639 (1993).
- [48] P. Laguna, V. Natchu, R. A. Matzner, and T. Vachaspati, Phys. Rev. Lett. **98**, 041602 (2007), hep-th/0604177.
- [49] M. Eto et al., Phys. Rev. Lett. **98**, 091602 (2007), hep-th/0609214.
- [50] E. Bogomol'nyi, Sov. J. Nucl. Phys. **24**, 449 (1976).
- [51] N. Turok, Phys. Rev. **D54**, 3686 (1996), astro-ph/9604172.
- [52] R. Durrer and M. Kunz, Phys. Rev. **D57**, 3199 (1998), astro-ph/9711133.
- [53] R. Durrer, M. Kunz, and A. Melchiorri, Phys. Rept. **364**, 1 (2002), astro-ph/0110348.
- [54] M. Doran, JCAP **0510**, 011 (2005), astro-ph/0302138, URL www.cmbeasy.org.
- [55] W. H. Press, B. S. Ryden, and D. N. Spergel, Astrophys. J. **347**, 590 (1989).
- [56] J. N. Moore, E. P. S. Shellard, and C. J. A. P. Martins, Phys. Rev. **D65**, 023503 (2002), hep-ph/0107171.
- [57] G. Vincent, N. D. Antunes, and M. Hindmarsh, Phys. Rev. Lett. **80**, 2277 (1998), hep-ph/9708427.
- [58] J. Urrestilla, A. Achucarro, J. Borrill, and A. R. Liddle, JHEP **08**, 033 (2002), hep-ph/0106282.
- [59] K. J. M. Moriarty, E. Myers, and C. Rebbi, Phys. Lett. **B207**, 411 (1988).
- [60] N. Bevis and M. Hindmarsh, *LATfield Web page* (2006), <http://www.latfield.org/>.
- [61] UK National Cosmology Supercomputer: SGI Altix 3700 containing 152×1.3 GHz Intel Itanium II CPUs, URL www.damtp.cam.ac.uk/cosmos/.
- [62] W. L. Freedman et al., Astrophys. J. **553**, 47 (2001), astro-ph/0012376.
- [63] D. Kirkman, D. Tytler, N. Suzuki, J. M. O'Meara, and D. Lubin, Astrophys. J. Suppl. **149**, 1 (2003), astro-ph/0302006.
- [64] R. A. Knop et al. (The Supernova Cosmology Project), Astrophys. J. **598**, 102 (2003), astro-ph/0309368.
- [65] G. Hinshaw et al. (WMAP), Astrophys. J. Suppl. **170**, 288 (2007), astro-ph/0603451.
- [66] W. Hu and M. J. White, Phys. Rev. **D56**, 596 (1997), astro-ph/9702170.
- [67] M. Kamionkowski, A. Kosowsky, and A. Stebbins, Phys. Rev. **D55**, 7368 (1997), astro-ph/9611125.
- [68] A. Lewis and S. Bridle, Phys. Rev. D **66**, 103511 (2002), astro-ph/0205436.
- [69] C.-l. Kuo et al. (ACBAR), Astrophys. J. **600**, 32 (2004), astro-ph/0212289.
- [70] W. C. Jones et al. (BOOMERANG), Astrophys. J. **647**, 823 (2006), astro-ph/0507494.
- [71] A. C. S. Readhead et al. (CBI), Astrophys. J. **609**, 498 (2004), astro-ph/0402359.
- [72] C. Dickinson et al. (VSA), Mon. Not. Roy. Astron. Soc. **353**, 732 (2004), astro-ph/0402498.
- [73] L. Page et al. (WMAP), Astrophys. J. Suppl. **170**, 335 (2007), astro-ph/0603450.
- [74] D. Parkinson, P. Mukherjee, and A. R. Liddle, Phys. Rev. D **73**, 123523 (2006), astro-ph/0605003.
- [75] A. R. Liddle, P. Mukherjee, and D. Parkinson, Astron. Geophys. **47**, 4.30 (2006), astro-ph/0608184.
- [76] M. Kunz, R. Trotta, and D. Parkinson, Phys. Rev. **D74**, 023503 (2006), astro-ph/0602378.
- [77] R. Trotta, Mon. Not. Roy. Astron. Soc. **378**, 819 (2007), astro-ph/0703063.
- [78] S. Cole et al. (The 2dFGRS), Mon. Not. Roy. Astron. Soc. **362**, 505 (2005), astro-ph/0501174.
- [79] W. J. Percival et al., Astrophys. J. **657**, 645 (2007), astro-ph/0608636.
- [80] A. G. Sanchez and S. Cole (2007), arXiv:0708.1517 [astro-ph].
- [81] C. Burrage and A. C. Davis, JHEP **06**, 086 (2007), arXiv:0705.1657 [hep-th].
- [82] C. Burrage and A. C. Davis, JHEP **11**, 023 (2007), 0707.3610.
- [83] P. M. Saffin, JHEP **09**, 011 (2005), hep-th/0506138.
- [84] M. Hindmarsh and P. M. Saffin, JHEP **08**, 066 (2006), hep-th/0605014.
- [85] A. Rajantie, M. Sakellariadou, and H. Stoica, JCAP **0711**, 021 (2007), 0706.3662.
- [86] J. Urrestilla and A. Vilenkin, JHEP **02**, 037 (2008), 0712.1146.
- [87] U. Seljak, U.-L. Pen, and N. Turok, Phys. Rev. Lett. **79**, 1615 (1997), astro-ph/9704231.
- [88] R. G. Crittenden and N. Turok, Phys. Rev. Lett. **75**, 2642 (1995), astro-ph/9505120.
- [89] R. Durrer, M. Gasperini, M. Sakellariadou, and G. Veneziano, Phys. Lett. **B436**, 66 (1998), astro-ph/9806015.